

COMAE: COMprehensive Attribute Exploration for Zero-shot Hashing

YUQI LI* and QINGQING LONG*, Computer Network Information Center, Chinese Academy of Sciences, China

NING CAO and SHUAI LIU, Nanyang Technological University, Singapore

XIAO LUO, University of California at Los Angeles, USA

ZHENG FANG and ZHIHONG ZHU, Peking University, China

ZHIYUAN NING, XUEZHI WANG[†], and YUANCHUN ZHOU, Computer Network Information Center, Chinese Academy of Sciences. University of Chinese Academy of Sciences, China

Zero-shot hashing (ZSH) has shown excellent success owing to its efficiency and generalization in large-scale retrieval scenarios. While considerable success has been achieved, there still exist urgent limitations. Existing works ignore the locality relationships of representations and attributes, which have effective transferability between seeable classes and unseeable classes. Also, the continuous-value attributes are not fully harnessed. In response, we conduct a COMprehensive Attribute Exploration for ZSH, named COMAE, which depicts the relationships from seen classes to unseen ones through three meticulously designed explorations, i.e., *point-wise*, *pair-wise* and *class-wise* consistency constraints. By regressing attributes from the proposed attribute prototype network, COMAE learns the local features that are relevant to the visual attributes. Then COMAE utilizes contrastive learning to comprehensively depict the context of attributes, rather than instance-independent optimization. Finally, the class-wise constraint is designed to cohesively learn the hash code, image representation, and visual attributes more effectively. Experimental results on the popular ZSH datasets demonstrate that COMAE outperforms state-of-the-art hashing techniques, especially in scenarios with a larger number of unseen label classes. Our source codes are available at <https://github.com/YihangZhou0424/NN2024-COMAE>.

CCS Concepts: • Computing methodologies → Visual content-based indexing and retrieval; • Information systems → *Image search*.

Additional Key Words and Phrases: Prototype Learning, Local Representation, Zero-shot Hashing, Image Zero-shot Hashing, Image Hashing, Image Retrieval.

ACM Reference Format:

Yuqi Li, Qingqing Long, Ning Cao, Shuai Liu, Xiao Luo, Zheng Fang, Zhihong Zhu, Zhiyuan Ning, Xuezhi Wang, and Yuanchun Zhou. 2024. COMAE: COMprehensive Attribute Exploration for Zero-shot Hashing. *ACM Trans. Multimedia Comput. Commun. Appl.* 1, 1, Article 1 (January 2024), 17 pages. <https://doi.org/XXXXXX>

*These authors contributed equally to this work.

[†]Corresponding author.

Authors' Contact Information: Yuqi Li, yuqili010602@gmail.com; Qingqing Long, qqlong@cnic.cn, Computer Network Information Center, Chinese Academy of Sciences, China; Ning Cao, s210089@e.ntu.edu.sg; Shuai Liu, Nanyang Technological University, Singapore, shuai004@e.ntu.edu.sg; Xiao Luo, University of California at Los Angeles, USA, xiaoluo@cs.ucla.edu; Zheng Fang, fang_z@pku.edu.cn; Zhihong Zhu, Peking University, China, zhihongzhu@stu.pku.edu.cn; Zhiyuan Ning, ningzhiyuan@cnic.cn; Xuezhi Wang, wxz@cnic.cn; Yuanchun Zhou, Computer Network Information Center, Chinese Academy of Sciences. and University of Chinese Academy of Sciences, China, zyc@cnic.cn.

Permission to make digital or hard copies of all or part of this work for personal or classroom use is granted without fee provided that copies are not made or distributed for profit or commercial advantage and that copies bear this notice and the full citation on the first page. Copyrights for components of this work owned by others than the author(s) must be honored. Abstracting with credit is permitted. To copy otherwise, or republish, to post on servers or to redistribute to lists, requires prior specific permission and/or a fee. Request permissions from permissions@acm.org.

© 2024 Copyright held by the owner/author(s). Publication rights licensed to ACM.

Manuscript submitted to ACM

Image hashing techniques have garnered substantial interest due to their remarkable efficacy in multimedia retrieval and content-based searches for images and documents [16, 18, 41]. Particularly, hashing techniques convert high-dimensional and complicated data into binary codes, which enables efficient searches in the binary Hamming space, thereby contributing to a smaller memory footprint and increased search efficiency [15, 20, 32]. The capability to depict intricate data in a compact binary format not only accelerates retrieval processes but also markedly improves storage efficiency. Consequently, image hashing emerges as a highly valuable asset in situations that necessitate swift and resource-efficient information retrieval.

With the popularity of content and social apps, the growth of Internet images leads to sort of new concepts, presenting a challenge for traditional hashing algorithms that struggle to adapt to unseen data in previously unobserved categories [23, 38, 41]. Recent researchers paid attention to the Zero-Shot Hashing (ZSH) issue. Visual attributes, pervasive across prevalent image datasets, serve to delineate discriminative visual properties intrinsic to objects, transcending specific classes and establishing a foundation for addressing the intricacies of previously unseen data [4, 17]. Notably, these attributes offer a robust representation for recognizing out-of-distribution samples, making them valuable for capturing similarities in the seen and unseen concepts in Zero-Shot Learning (ZSL) tasks [2, 45]. Fig. 1 shows an example of the class-level attributes. Nevertheless, the exploration of visual attributes within the realm of ZSH tasks has been relatively meager. AH [45] adopts a straightforward approach by constructing a multi-task architecture to capture the intricate relationships between visual attributes and category classes, thereby facilitating the transfer of knowledge.

While considerable success has been achieved in utilizing visual attributes to establish connections among visual attributes, image features, class labels, and binary hash codes, there still exists urgent limitations [20, 45]. Firstly, image locality representations are proven to be critical to zero-shot learning tasks [19], as the locality exhibits more effective transferability between seen classes and unseen classes. However, existing works ignore the locality representations in deep hashing tasks, which decreases the upper bound of the transferability in hashing algorithms. Secondly, existing works mainly focus on individual image representation learning, optimizing each instance independently. Each dimension of the visual attribute is a continuous value. In contrast to the binary one-hot class encoding, these continuous values encompass richer and more nuanced distance-related information. These informative attributes are aptly poised to capture intricate pairwise relationships, while they are largely ignored by prevailing works. Thirdly, existing works generally employ a multi-task learning framework to independently utilize attribute labels and class labels. Yet their actual relationships are more complicated than such simple presumes. To be specific, two images may belong to the same class but pose disparate attributes. For example, two images with a “bird” class may have “black leg” and “yellow leg”. Similarly, instances with different classes may also exhibit sharing analogous attributes. For example, two images with “bird” and “wapiti” classes may have the same “black leg”. The existing methods may not lead to the global optimum, thus necessitating performing joint optimization to achieve the overall optimum for both tasks.

To tackle the above issues, we conduct a **COM**prehensive **A**ttribute **E**xploration for zero-shot hashing, named **COMAE**. It combines relationships among visual attributes, image features, class labels, and binary hash codes. Specifically, we develop a supervised learning objective that localizes visual attributes for point-wise consistency. By utilizing the attribute prototype network, we aim to capture the fine-grained details and distinctive characteristics of images, enabling more accurate and informative hash codes. To comprehensively harness numerical attribute features, we construct positive and negative instances for each image based on the numerical disparities of attributes and utilize contrastive learning to further model their distance relationships. Thus, our model can capture the subtle variations in attribute values across different images and learn representations that encode the common visual characteristics associated with these attributes. Finally, class-wise optimization is proposed to cohesively learn the hash code, image

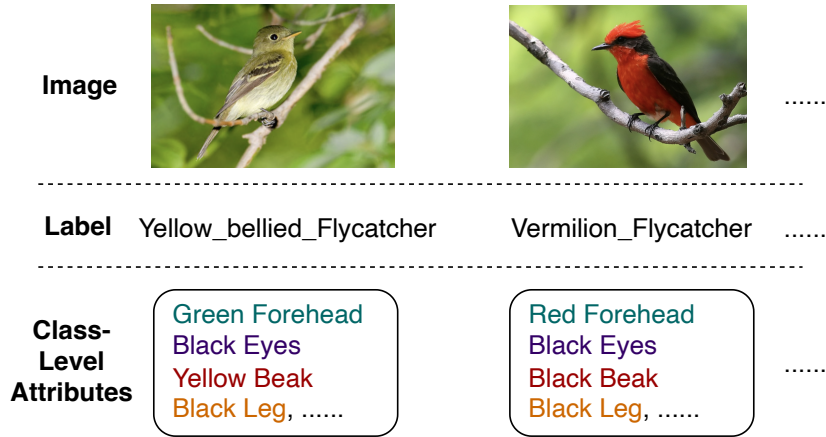


Fig. 1. An example of the class-level attributes.

representation, and visual attributes more effectively, which fosters improved generalization by considering the relationships and dependencies between different classes during the learning process. We jointly learn discriminative global and local features based on the class-level attributes. Extensive experiments on the ZSH benchmark datasets show that COMAE outperforms the state-of-the-art methods, especially in scenarios with a larger number of unseen label classes. It serves to validate the effectiveness of comprehensive attribute explorations.

Our contributions are summarized as follows:

- We conduct a COMprehensive Attribute Exploration for zero-shot hashing, named COMAE, it depicts the relationships between seen classes and unseen classes through three meticulously designed explorations, i.e., point-wise, pair-wise and class-wise consistency constraints.
- We design an attribute prototype network, a contrastive learning unit, and a joint-optimal label utilization to implement the above three components.
- Experiments on three popular zero-shot hashing datasets show that COMAE significantly outperforms the state-of-the-art methods, especially in scenarios with a larger number of unseen label classes.

This paper is generally organized as follows. We begin with briefly reviewing related works in Section 2. Then the proposed COMAE is technically introduced in Section 3. We provide extensive experiment results and discussions in Section 4. Finally, we conclude this work in Section 5.

1 Related Work

1.1 Deep Hashing

Image hashing is a popularly used method for approximating nearest neighbor search in large-scale retrieval scenarios [38]. Shallow image hashing methods often leverage handcrafted features or employ traditional machine-learning algorithms to generate compact binary representations. Typical works include LSH [1] and ITQ [10]. Shallow methods are computationally efficient and exhibit simplicity in their design, yet they may struggle to capture complex and high-level semantic features inherent in images.

Over the past decades, deep learning models have shown excellent progress in the field of Computer Vision [17, 27] and Natural Language Processing [23, 33], many scholars pay attention to leveraging deep neural networks to learn the abstract representations. Deep hashing methods can be achieved through three paths. The first path utilizes limited information, which has a lower upper bound of the capability. ASZH [32] is a typical work in the first path, that learns hash functions based on the seeable category labels, for generating binary codes for unseeable data. The second path [11, 49] generates semantic vectors based on the visual attributes to find a semantic embedding space, then transfers the common knowledge to unseeable classes. TSK, SitNet, and OPZH [11, 46, 49] are representative semantic-based works, they conduct a multi-task framework in which the class labels and attribute vectors are co-trained through the hashing network, and the labels are projected into a semantic embedding space. However, there exists an inherent gap between the semantic and visual space, and the alignment of spaces is tough. The third path [45] constructs relationships among attributes, image features, binary codes, and class labels. These models are considered to be more generalized when dealing with out-of-distribution and open-set samples [2, 9].

1.2 Zero-shot Learning

Zero-shot learning (ZSL) [8, 22, 44, 51] is designed to extend object recognition across known and unknown classes via a unified embedding space, where both categories are described by their semantic visual identifiers. Early ZSL methods [8, 27] harvest global visual features from networks, whether pre-trained or capable of end-to-end training. Typically, end-to-end frameworks often surpass pre-trained ones by refining visual attributes, thus mitigating biases between the datasets used for training and those for ZSL applications. Nonetheless, such strategies typically produce less than ideal outcomes [44], as they struggle to discern the subtle variances between seen and unseen categories. Recent innovations in ZSL predominantly concentrate on methods based on attention [36, 44, 51], employing visual attributes to identify distinct feature regions, for instance, specific parts of a bird. This emphasis highlights the critical roles of specificity and the arrangement of image features in ZSL. Proposals for prototype networks [36] strive to pinpoint various attributes within images to bolster the precision of feature localization. Inspired by these insights into visual attributes and the delicate distinctions between recognized and unrecognized classes, our methodology adopts the prototype network to intricately map the relationships between visual attributes and hash codes [44].

1.3 Contrastive Learning

Contrastive learning aims at honing representations by juxtaposing similar instance pairs (positive pairs) against dissimilar ones (negative pairs) [12, 13], enhancing the model's ability to differentiate between closely related and distinct instances effectively. Many works demonstrate that contrastive learning is able to alleviate the problems of numerous categories and imbalanced class distributions. In addition, it can amplify the subtle distinctions among similar classes, which assists in capturing intricate details that are often overlooked by basic models. [12] is the first attempt work to improve learned representations by contrasting positive and negative pairs. SimCLR [5] utilizes a self-supervised learning architecture that substitutes the conventional memory bank with batch-specific elements, significantly enhancing its performance on the ImageNet dataset. As hash code is a form of representation, recent researches [28, 34, 47] take attempts to utilize contrastive learning in deep hashing. [47] proposes weighted contrastive hashing to explore the fine-grained semantic relations among images. [34] propose to However, random sampling could result in augmented images with different semantics, deteriorating the performance of contrastive learning.

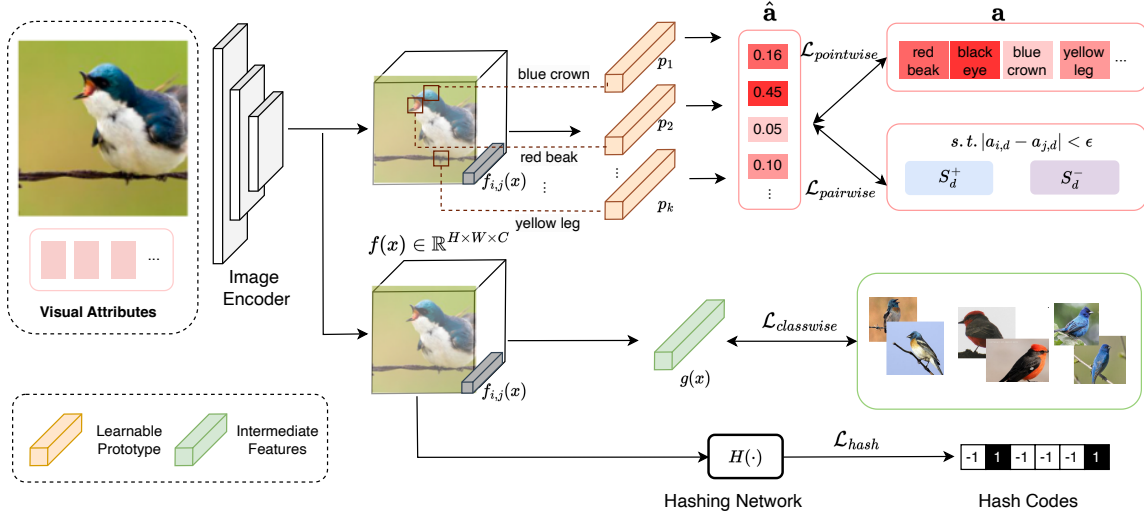


Fig. 2. The architecture of the proposed COMAE. It consists of three modules: a) Point-wise objective aims at improving image locality and attribute representations; b) Pair-wise loss is proposed to learn the representations from individual learning to context-based learning; and c) Class-wise constraint is designed to capture relationships of attributes and class labels.

2 Method

The architecture of the proposed COMAE is shown in Fig. 2. Our proposed COMAE depicts the relationships between seen and unseen classes through three meticulously designed explorations, i.e., point-wise, pair-wise, and class-wise consistency constraints. To improve the image locality and attribute representations, we propose a point-wise objective. To learn the representations from individual learning to context-based learning, we utilize contrastive learning to build pair-wise loss. For capturing relationships between attributes and class labels, a class-wise constraint is designed.

2.1 Problem Definition

Let $X = \{x_i\}_{i=1}^N \in \mathbb{R}^{N \times H \times W \times C}$ be N images, where H, W, C denote the image height, width, and channel. The matrix $Y = \{y_i\}_{i=1}^N \in \mathbb{R}^{N \times C}$ is the label matrix, where C denotes the number of classes. The classes are divided into the seeable class Y^s and the unseeable class Y^u , where $|Y^s| \cup |Y^u| = |C|$, $|Y^s| \cap |Y^u| = \emptyset$. Let $A = \{a_i\}_{i=1}^N \in \mathbb{R}^{N \times K}$ denote the class-level attribute vector in K dimensions. By using training samples which contain labeled images and attributes from seeable classes, i.e., $S = \{x, y, a | x \in X, y \in Y^s, a \in A\}$, we aim to learn a hashing model $\mathcal{H}: X \rightarrow b_i \in \{-1, 1\}^l$, where b_i represents the learned l -bit binary hash codes. In the testing process, attribute vectors of unseen classes are also known. In this paper, zero-shot hashing focuses on predicting the hashing label of images from unseen classes, i.e., $X \rightarrow Y^u$.

2.2 Point-wise Attribute Consistency

Image locality representations are proven to be practical in transferring knowledge from seen to unseen classes [19, 44]. For more subtly depicted image and attribute characterizations, we first conduct point-wise consistency constraint, which takes the attribute regression loss as the supervision. Prototype learning has proven to be robust in dealing with

open-set recognition and out-of-distribution samples [37, 44] in recent years. In the prototype learning scheme, each category is represented by a prototype. This prototype can be the mean of the sample in the category, the center of mass, or some other representative sample. Thus we introduce a prototype module aiming at capturing the relationships of local features and visual attributes.

Let $f_{i,j}(x) \in \mathbb{R}^C$ denote the image representation at spatial position (or location) (i, j) . It depicts the information on local image regions. Then we learn sorts of attribute prototypes $P = \{p_k \in \mathbb{R}^C\}_{k=1}^K$ to predict attributes from the local visual characterizations. Let p_k denote the learnable prototype embeddings for the k -th attribute. As shown in Fig. 2, p_1 and p_2 correspond to the prototypes for “red beak” and “yellow leg” respectively. For each attribute, we produce a similarity map $M^k \in \mathbb{R}^{H \times W}$, where each element is computed by a non-linear network $\Theta(\cdot)$ between p_k and each local feature. To associate each visual attribute with its closest local feature, we gain the predicted k -th attribute \hat{a}_k by taking the maximum value in the similarity map M^k ,

$$\begin{aligned} M_{i,j}^k &= \Theta(p_k, f_{i,j}(x)), \\ \hat{a}_k &= \max_{i,j} M_{i,j}^k. \end{aligned} \quad (1)$$

This prototype captures the common characteristics of the category and plays a key role in the expression of the entire category. The visual attribute vectors supervise the learning of attribute prototypes. We formalize the attribute prediction task as a regression problem and then minimize the Mean Square Error (MSE) between the ground truth attributes and the predicted attribute score \hat{a} . By optimizing the regression objective, we enforce the local features to encode pivotal semantic attributes, improving the locality of representations, and further improving the quality of hashing codes,

$$\mathcal{L}_{\text{pointwise}} = \sum_i^N \frac{1}{N} \|a_i - \hat{a}_i\|^2. \quad (2)$$

Furthermore, we refine the similarity map to intensively focus on its peak region. To achieve this, we employ a compactness regularizer [50] on each similarity map M^k , ensuring a concentrated similarity assessment. The equation is defined as,

$$\mathcal{L}_{\text{reg}} = \sum_k^K \sum_h^H \sum_w^W M_{i,j}^k [(i - \tilde{i})^2 + (j - \tilde{j})^2], \quad (3)$$

where $(\tilde{i}, \tilde{j}) = \arg \max_{i,j} M_{i,j}^k$ identifies the coordinate with the highest value in M^k , which ensuring the attribute prototype mirrors only a minimal subset of local features, thus achieving a more streamlined similarity map. This method emphasizes the precision in the prototype’s focus, leading to a denser representation of similarity. Then the $\mathcal{L}_{\text{pointwise}}$ is changed to $\mathcal{L}_{\text{pointwise}} = \sum \frac{1}{N} \|a_i - \hat{a}_i\|^2 + \mathcal{L}_{\text{reg}}$. The effective representations of image locality ensure a more robust and versatile transfer of knowledge, contributing to the overall effectiveness of COMAE.

2.3 Pair-wise Attribute Consistency

To make full use of the limited yet crucial pieces of information, we conduct pair-wise attribute exploration to depict the context relationships of continuous-valued attributes. Recent studies proved that contrastive learning can enhance the discriminative capability of feature representations and enable the establishment of meaningful relationships between seen and unseen classes [6, 13, 28]. The fundamental concept of pairwise loss revolves around learning feature representations by comparing the similarity between different pairs of samples. The pairwise loss function enhances the model’s ability to compare sample pairs across these groups, directing it to recognize that samples within the same

category should exhibit higher similarity compared to those from different categories. This approach ensures a more discerning and category-aware similarity assessment within the model's learning process. Thus we utilize contrastive learning in the pair-wise constraint. We begin with constructing the positive sample set $S_d^+(i)$ of the i -th image and the negative sample set $S_d^-(i)$ in the d -th dimension of all attributes. Specifically, given the attribute of i -th image, which denoted as a_i , we build the positive set of i -th image as follows,

$$S_d^+(i) = \{j \mid |a_{i,d} - a_{j,d}| < \epsilon, j \neq i, j = 1, \dots, N\}, \quad (4)$$

where ϵ is a hyper-parameter and is set through multiple experiments. We randomly sample k negative samples for the i -th image, as considering all negative samples will bring high complexity. We get the sample set $S_d(i) = S_d^+(i) \cup S_d^-(i)$. Afterwards, we formulate the attribute-level contrastive embedding objective as follows,

$$\mathcal{L}_{\text{pairwise}} = - \sum_d^D \sum_i^N \frac{1}{DN} \log \frac{\sum_{j \in S_d^+(i)} \exp(\hat{a}_i \hat{a}_j / \tau)}{\sum_{t \in S_d(i)} \exp(\hat{a}_i \hat{a}_t / \tau)}, \quad (5)$$

where $\tau > 0$ is the temperature parameter. The attribute-level contrastive learning relies on attribute-wise supervision to enhance the discriminative ability in the new attribute space.

2.4 Class-wise Attribute Exploration

Class-wise attribute exploration aims to leverage image attributes to enhance the performance of classification. Compared with pointwise and pairwise explorations, it focuses on higher-level relationships of images and attributes. For high-level image representations, we adopt a global average pooling over the input image to learn a global discriminative feature $g(x) \in \mathbb{R}^C$, $g(x) = \frac{1}{HW} \sum_{i=1}^H \sum_{j=1}^W f_{i,j}(x)$. Subsequently, a linear layer employing parameter $W \in \mathbb{R}^{C \times K}$ maps the visual feature $g(x)$ into the designated class embedding space (e.g., attribute space). Calculating the dot product between this transformed visual feature and each class embedding generates class logits. This process is complemented by applying a cross-entropy loss function, which is designed to maximize the compatibility score between the image and its corresponding attribute vector, fostering a more accurate attribute-based classification,

$$\mathcal{L}_{\text{ce}} = - \frac{1}{|Y^s|} \sum_{y_i \in Y^s} \log \frac{\exp(g(x_i)^T W a_i)}{\exp(g(x_i)^T W \hat{a}_i)}, \quad (6)$$

The attribute embedding layer and image representations are jointly optimized, with class labels directing the overall optimization effort. Note that the attribute prototypes, which facilitate the transfer of knowledge from seen to unseen classes, are shared across different classes. This sharing mechanism enhances image representation for zero-shot learning, improving the model's ability to generalize to new, unseen classes.

2.5 Hashing Learning

After conducting the above three consistency constraints, the image representations can contain more comprehensive attribute and class relationships. In this section, we derive a hash network based on the improved representations. Denote our hashing network as $H(\cdot)$, given an input image representation $f(x)$ from the pre-trained image encoder $f(\cdot)$. We take the Fully Connected Hash (FCH) as the fully connected layer in $f(\cdot)$ for generating binary code $b_i \in \mathbb{R}^d$,

by binarization process with the use of sign function. The process is formulated as follows,

$$b_i = \text{sign} \left(\sum_{c=1}^C \sum_{h=1}^H \sum_{w=1}^W f(x_i) W_{h,w,c} \right), \quad (7)$$

where $W_{h,w,c}$ is the learnable transform matrix. It changes the last fully connected layer to a d -dimension representation.

To compress intra-class hashing code with strong constraints, we use the hypersphere loss [21, 40] to optimize the FCH layer with large angular boundaries between classes. The spherical hashing objective offers several advantages within the context of similarity-preserving hash coding. One notable advantage lies in its ability to enforce constraints on binary codes such that they reside on a hypersphere in the Hamming space. This geometric constraint enhances the discriminative power of the learned hash codes by facilitating a more structured and separable representation of data points. Additionally, the hypersphere constraint promotes semantic similarity preservation, as points closer to the hypersphere correspond to more semantically similar items. This results in improved retrieval performance, particularly in scenarios where maintaining semantic relationships among binary codes is crucial, such as image retrieval and nearest neighbor search. Furthermore, the geometric regularity induced by the hypersphere constraint contributes to robustness against noise and variations, thereby enhancing the overall effectiveness and stability of the hashing model. It is defined as,

$$\mathcal{L}_{\text{hash}} = -\frac{1}{N} \sum_i^N \log \left(\frac{e^{\|b_i\| \psi(\theta_{y_i, i})}}{e^{\|b_i\| \psi(\theta_{y_i, i})} + \sum_{j \neq y_i} e^{\|b_i\| \cos(\theta_j, i)}} \right), \quad (8)$$

$$\psi(\theta_{y_i, i}) = (-1)^k \cos(m\theta_{y_i, i}) - 2k,$$

where $m \geq 1$ is an integer that controls the size of the angular margin, and $\theta_{y_i, i} \in [\frac{k\pi}{m}, \frac{(k+1)\pi}{m}]$, $k \in [0, m-1]$. Compared with other hashing methods, it can achieve a larger separation and a smaller variation of inter-classes.

For a comprehensive exploration between the attribute learning and image hashing tasks, the **overall objective** is formalized as follows,

$$\mathcal{L} = \sum \lambda_i \mathcal{L}_i, \quad (9)$$

where \mathcal{L}_i denotes the pointwise-, pairwise-, and classwise-losses respectively, and λ_i denotes hyper-parameters. The parameters of the hashing network could not be updated by the standard back-propagation as the derivation of $\text{sign}(\cdot)$ is indifferentiable at zero. To solve this issue, the $\tanh(\cdot)$ function is adopted to approximate the results of $\text{sign}(\cdot)$. In this manner, we can optimize the original indifferentiable loss by the mini-batch Stochastic Gradient Descent (SGD).

3 Experiments

In this section, we will outline the experimental setups and provide a detailed discussion of our results. Our experiments are designed to answer the following questions (**RQ**):

- **RQ1:** Can the proposed COMAE gain superior performance in comparison to other baselines?
- **RQ2:** How does the performance of COMAE evolve in response to the change in the ratio of unseen classes in the training process?
- **RQ3:** What insights can be derived from an ablation study conducted on the proposed approach?
- **RQ4:** How does the performance of COMAE evolve in response to the change of hyper-parameters?

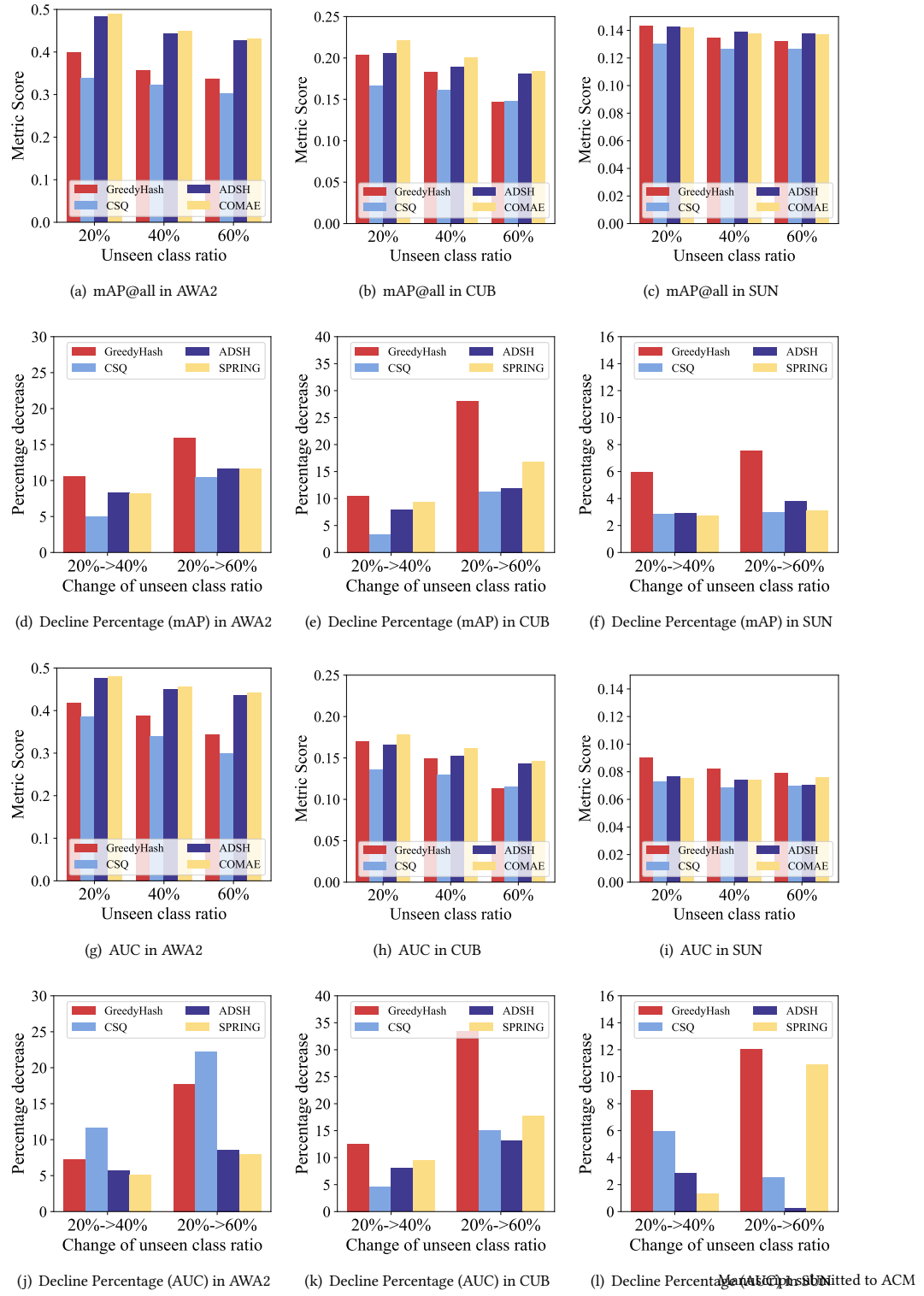


Fig. 3. mAP@all and AUC scores and their decline percentage with the change of unseen classes ratio in the training process.

Table 1. The mAP@5000 results on three popular ZSH datasets in different code lengths.

Methods	AWA2				CUB				SUN			
	24 bits	48 bits	64 bits	128 bits	24 bits	48 bits	64 bits	128 bits	24 bits	48 bits	64 bits	128 bits
LSH	0.0106	0.0151	0.0204	0.0306	0.0055	0.0069	0.0076	0.0095	0.0598	0.0738	0.0764	0.0880
SH	0.1833	0.2729	0.2955	0.3441	0.0568	0.081	0.0886	0.1191	0.0738	0.0811	0.0837	0.0880
ITQ	0.1999	0.2821	0.2964	0.3764	0.0533	0.0765	0.0892	0.1182	0.0725	0.0899	0.0918	0.1007
IMH	0.1282	0.1536	0.1613	0.1681	0.0330	0.0361	0.0364	0.0386	0.0572	0.0668	0.0638	0.0651
PCA	0.2165	0.2530	0.2701	0.2719	0.0547	0.0598	0.0632	0.0695	0.0808	0.0868	0.0891	0.0980
HashNet	0.2086	0.2386	0.2516	0.2749	0.0528	0.0566	0.0595	0.0633	0.0746	0.0825	0.0865	0.0944
GreedyHash	0.3420	0.4169	0.4240	0.4639	0.1132	0.1707	0.1841	0.2326	0.0873	0.1259	0.1398	0.1550
JMLH	0.3607	0.4364	0.4408	0.4711	0.1078	0.1555	0.1987	0.2310	0.0860	0.1168	0.1345	0.1500
ADSH	0.3360	0.4787	0.5105	0.5454	0.0858	0.1607	0.1827	0.2424	0.0886	0.1230	0.1341	0.1731
CSQ	0.3194	0.3988	0.3773	0.4072	0.0996	0.1588	0.1712	0.2201	0.0915	0.1211	0.1375	0.1669
DPN	0.1783	0.2086	0.2378	0.2565	0.0445	0.0728	0.0772	0.1003	0.0737	0.0825	0.0894	0.1126
BiHalf	0.3440	0.4036	0.4223	0.4577	0.0794	0.1280	0.1573	0.2142	0.0077	0.0490	0.0512	0.1307
OrthoCos	0.1709	0.2302	0.2312	0.2566	0.0451	0.0660	0.0736	0.0984	0.0728	0.0809	0.0868	0.1126
CIBHash	0.2113	0.2304	0.2481	0.2618	0.0351	0.0404	0.0411	0.0453	0.0690	0.0808	0.0809	0.0883
TBH	0.0941	0.1201	0.1073	0.1730	0.0157	0.0176	0.0226	0.0252	0.0169	0.0230	0.0248	0.0287
TSK	0.2262	0.3109	0.3873	0.4151	0.0739	0.1200	0.1394	0.1112	-	-	-	-
ASZH	0.2619	0.3787	0.4032	0.4158	0.0764	0.1192	0.1294	0.1727	-	-	-	-
SitNet	0.2344	0.2406	0.2549	0.2650	0.0880	0.1127	0.1141	0.1167	-	-	-	-
OPZH	0.1056	0.1390	0.1618	0.1961	0.0632	0.0879	0.0962	0.1143	-	-	-	-
AH	0.2275	0.1989	0.3154	0.3557	0.0480	0.0897	0.1089	0.1445	-	-	-	-
COMAE	0.3819	0.4792	0.5133	0.5465	0.1136	0.1777	0.1994	0.2519	0.0923	0.1264	0.1415	0.1741

3.1 Experimental Settings

3.1.1 Datasets. In our investigations, we meticulously analyzed three distinguished zero-shot hashing datasets referenced in [32], i.e., AWA2 [43], CUB [39], SUN [26]. AWA2 encompasses 37,322 images across 50 animal categories, with a configuration of 40 seen and 10 unseen classes, each described by 85 attributes [39]. The CUB dataset includes 11,788 images from 200 bird species, categorized into 150 seen and 50 unseen classes, each characterized by 312 attributes. SUN dataset, on the other hand, contains 14,340 images from 717 scene categories, with a division of 645 seen and 72 unseen classes, each depicted by 102 attributes.

3.1.2 Baselines. We select the following representative image hashing baselines as our competitors:

- **Image Shallow Hashing** methods often leverage handcrafted features or employ traditional machine-learning algorithms to generate compact binary representations. Typical works include LSH [1], SH [42], ITQ [10], SDH [29], IMH [30], and PCA [25]. Shallow methods are computationally efficient and exhibit simplicity in their design, yet they may struggle to capture complex and high-level semantic features inherent in images.
- **Image Deep Hashing** methods, leverage deep neural networks to automatically learn hierarchical and abstract representations of images. Representative works can be categorized into two paths, supervised hashing works, i.e, HashNet [3], GreedyHash [35], JMLH [31], ADSH [52], CSQ [48], DPN [7], OrthoCos [14], and unsupervised hashing works, i.e, BiHalf [20], TBH [28], CIBHash [28]. By employing end-to-end learning, deep hashing methods aim to optimize hash codes directly from raw pixel values, allowing for the discovery of intricate and discriminative image representations.

- **Zero-shot Image Hashing** methods extend the above algorithms to handle scenarios where the model encounters classes during testing that were not seen during training. These methods often incorporate semantic information, such as image attribute descriptions, or meta-learning strategies to enhance the model’s adaptability to unseen classes. Representative works include TSK [46], ASZH, SitNet, OPZH, and AH. ASZH [32] uses category labels to learn the hash functions from the seen training data, to generate binary codes for unseen data. SitNet [11], and OPZH [49] adopt semantic vectors to find semantic embedding space for knowledge transferability. AH [45] constructs relationships and image features for transferability.

3.1.3 Evaluation Metric. For evaluating different aspects of our study, we employed a variety of metrics. These include the mean Average Precision (mAP) and the Area Under the Precision-Recall Curve (AUC) for assessing the ranking quality of search outcomes. Specifically, we present findings for the top 5,000 samples and for the entire dataset, denoted as mAP@5000 and mAP@all, respectively. Additionally, we utilized four conventional metrics: mean Average Precision (mAP), Precision-Recall Curve (PR Curve), Precision@N Curve (P@N Curve), and Recall@N Curve (R@N Curve), with a particular focus on the ranking performance for the initial 5,000 retrieved samples.

3.1.4 Implementation Details. All comparative baselines are conducted with their default hyper-parameter configurations. For a fair comparison, their image feature extractors are substituted with the ResNet101 [17]. The training epoch is set to 10 and the batch size is set to 64, and more than 10 will be overfitting, resulting in a decrease in accuracy. We take Adam as the optimizer weight decay 0.0005 and the learning rate is set to 0.0001. The ϵ in Eqn. 9 is set to 0.9, the λ_1 , λ_2 , and λ_3 in Eqn. 4 are set to 10, 1, and 10 respectively. To ensure the statistical significance of our experimental data, the average outcomes of each technique were calculated based on ten iterations.

3.2 RQ1: Overall Performance

Table. 1 displays the results of the COMAE and all competitive baselines on datasets AWA2, CUB, and SUN with hash code lengths of 24, 48, 64, and 128. Note that the source codes of ASZH, SitNet, AH, and OPZH are unavailable, thus we use their results in paper [32]. The experimental settings of Table 1 are the same as [32]. In Fig. 4, we illustrate three distinct curves, i.e., PR Curve, R@N Curve, and the P@N Curve, to evaluate the performance of hash codes with a length of 64 bits on all datasets. Typically, the efficacy of a method is gauged by the PR curve approaching the upper right quadrant, with higher positions on the P@N and R@N curves indicative of superior performance. Overall, we find the following conclusions,

- As shown in Table. 1, deep hashing models perform better than shallow hashing ones in general, which shows the superiority of neural networks. In addition, The zero-shot hashing models exhibit superior performance in comparison to both deep and shallow hashing models.
- COMAE surpasses all existing zero-shot hashing benchmarks, in terms of all bit lengths. At the same time, the performance of COMAE remains relatively stable when the number of bits increases. Compared with AH [45], an attribute-based zero-shot hashing method, we gain better performance, which serves to validate the correctness and effectiveness of the motivation we put forth.
- An insightful observation can be derived from the graphical representation in Fig. 4 in all datasets. COMAE attains a heightened accuracy at a comparatively lower recall rate, thereby demonstrating the superiority of our proposed method.

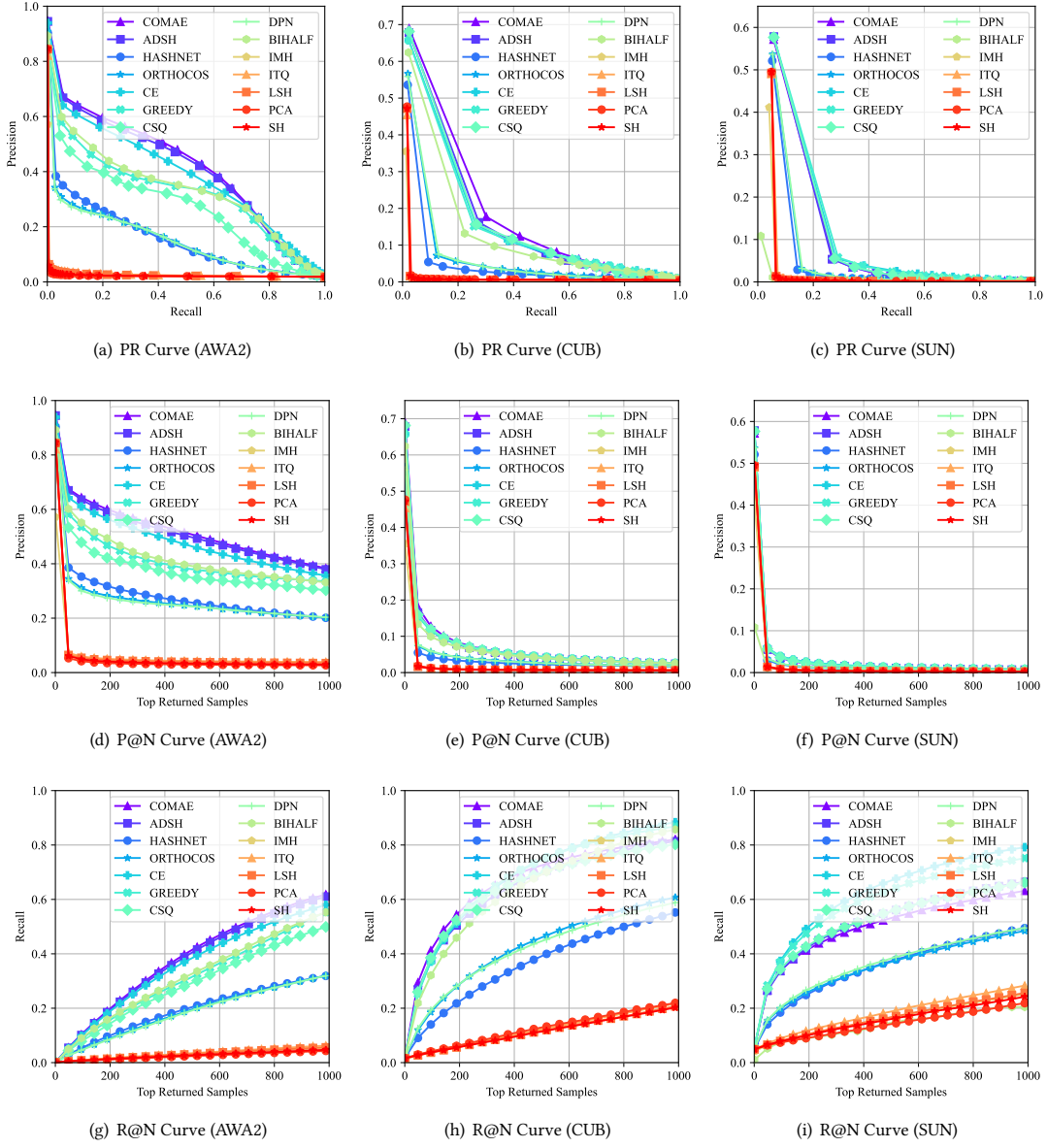


Fig. 4. The comparison of PR Curve, P@N Curve and R@N Curve in 64 bit length codes.

3.3 RQ1: Hashing Code Visualization

In this experiment, we adopted a more intuitive approach to visualizing hashing codes to evaluate the effectiveness of our proposed COMAE. Throughout the comparative experiments, we initially transformed the 64-bit hashing codes into lower-dimensional spaces, subsequently projecting these codes into a 2-D plane using the t-SNE [24] tool.

Manuscript submitted to ACM

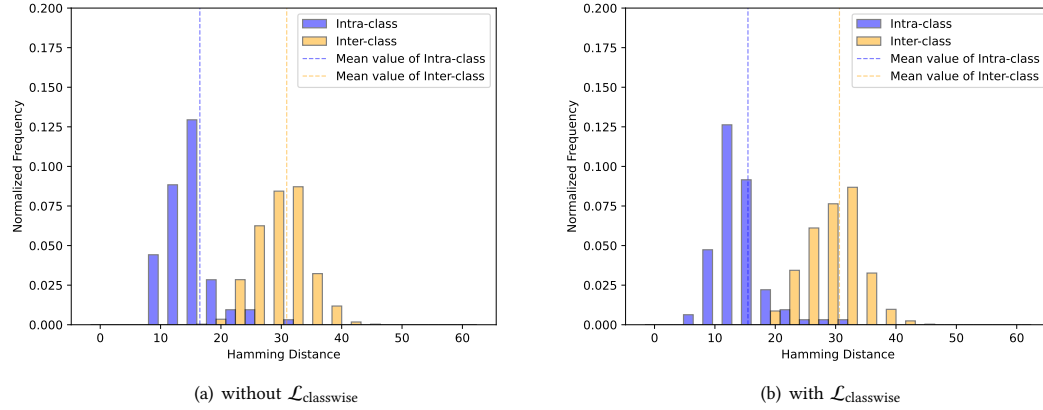


Fig. 5. Histogram distances of the intra-classes and inter-classes. The arrow annotation is the quantitative separability with the hamming distance, $\mathbb{E}[D_{inter}] - \mathbb{E}[D_{intra}]$.

This methodology facilitated a clearer observation of COMAE’s performance through visual means. We present the visualization of hash code for all testing samples with unseen classes on the AWA2 dataset. Results are shown in Fig. 7. According to the visualization results, we find that a) HashNet, DPN and OrthoCos perform badly, which are unable to distinguish the unseen classes. b) Although CSQ and BiHalf gain favorable outcomes in visualization and mAP@5000 results in Table. 1, they still encounter challenges such as substantial inter-class overlap and indistinct boundaries (the classes represented by the green and other colors). c) Compared with other baselines, the proposed COMAE achieves the best performance, as the generated hash codes are more distinguished. It indicates that COMAE can effectively classify images.

3.4 RQ2: Effects of Unseen Class Ratio

To verify the robustness of our model in the context of the zero-shot scenario, we conduct experiments where the number of seen class categories underwent a progressive reduction during the training process. The results are visually depicted in Fig. 3. Specifically, (d)-(f) and (j)-(l) show the performance decrease ratio between 20%→40% and 20%→60% respectively. We conclude the following conclusions based on the outcome results,

- All deep hashing methods manifest a discernible decline in performance concomitant with an escalation in the number of unseen classes on three datasets. Notably, this performance deterioration not only intensifies but also amplifies in magnitude, as evidenced by both the *MAP@all* and *AUC* metrics.
- COMAE exhibits a performance superiority across various unseen class ratios, along with the most minimal decrease.

3.5 RQ3: Distance Visualization of Intra and Inter Classes

To verify whether the classwise constraint can broaden the distance of inter-class and reduce the distance of intra-class, we provide a quantitative comparison of the distance between the mean value of intra-class distances and inter-class distances, under the setting of without loss $\mathcal{L}_{contrastive}$ and with the loss. Fig. 5 summarizes the histogram of intra-class

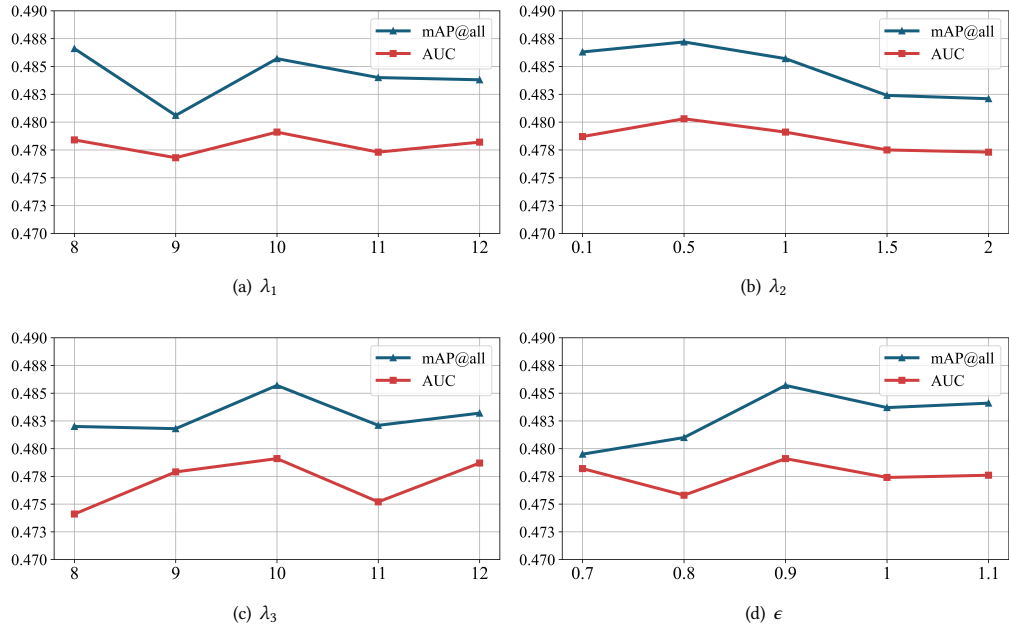


Fig. 6. The effects of hyper-parameters on AWA2 dataset.

and inter-class distances on the AWA2 dataset. We adjust the frequency normalization so the total of all histogram bins equals one. The directional marker indicates the separability in Hamming distances, $\mathbb{E}[D_{inter}] - \mathbb{E}[D_{intra}]$. Despite similar distributions for inter-class distances, the distinction between the average intra-class distance (indicated by the purple dotted line) and the average inter-class distance (shown by the orange dotted line) in scenario (b) exceeds that in scenario (a). This approach visually emphasizes the effect of the classwise constraint on class separability metrics. Quantificationally, the difference in (a) is 14.38, and the difference in (b) is 15.50. The results show that our proposed classwise constraint can enlarge the distance of the inter-class and reduce the distance of the intra-class.

3.6 RQ3: Component Analysis

To provide further insight into COMAE, we conduct component analysis on AWA2 and CUB datasets with 64-bit hashing-code lengths. We configure several variants of COMAE as a) COMAE-V1 is the COMAE model without $\mathcal{L}_{pointwise}$; b) COMAE-V2 represents the COMAE without $\mathcal{L}_{pairwise}$; c) COMAE-V3 refers to the COMAE without $\mathcal{L}_{classwise}$. Results are shown in Table 2. Compared with other components, the pointwise objective plays the most significant role in AWA2, and the pairwise objective in CUB. Also, the performance of COMAE on both datasets surpasses that of variants, validating the necessity of each component.

3.7 RQ4: Parameter Analysis

We analyze the impact of critical hyper-parameters, i.e., $\lambda_1, \lambda_2, \lambda_3$ that influence the weight of the auxiliary losses in Eqn. 9 and the threshold ϵ for selecting positive samples in Eqn. 4. These evaluations were performed using the AWA2 dataset with 64-bit hash codes, and the results are detailed in Fig. 6. As the increase of hyper-parameters, the

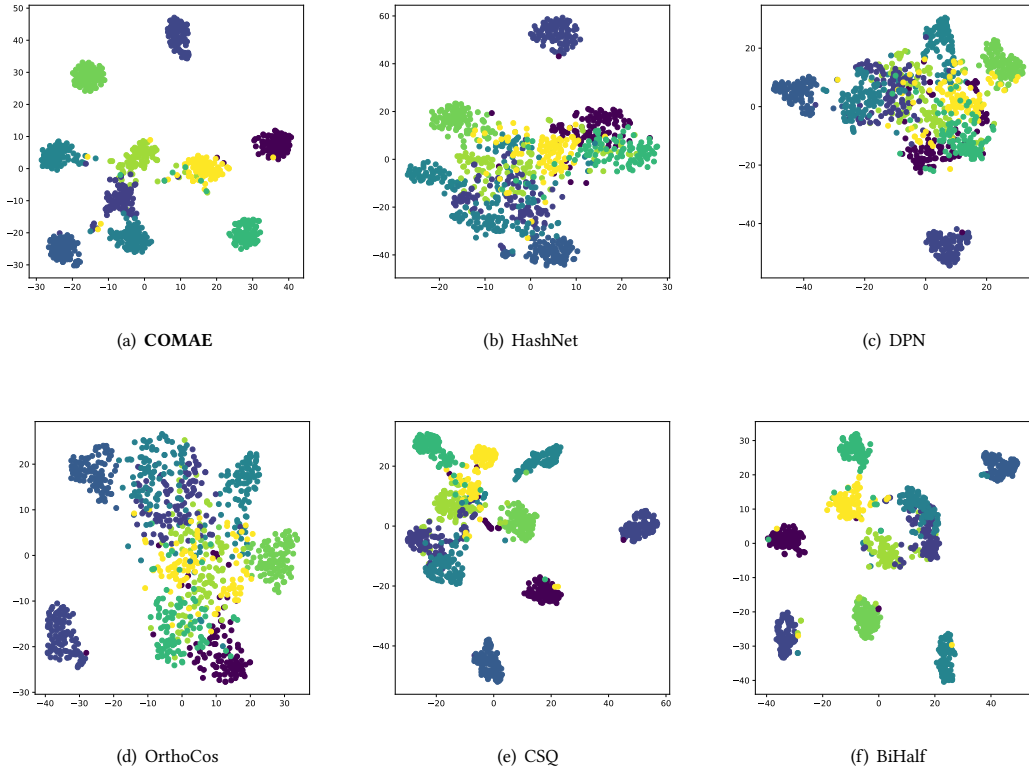


Fig. 7. t-SNE visualizations of hashing code on test unseen classes. The 10 colors denote 10 different unseen classes.

Table 2. The mAP@all and AUC results with switching model components in different datasets.

	AWA2		CUB	
	mAP@all	AUC	mAP@all	AUC
COMAE-V1	0.4830	0.4781	0.2069	0.2418
COMAE-V2	0.4857	0.4791	0.1867	0.2240
COMAE-V3	0.4835	0.4782	0.2064	0.2412
COMAE	0.4883	0.4812	0.2094	0.2416

performance of our model initially rises and then decreases. Hence, we choose the best hyper-parameters corresponding to the point at peak performance.

4 Conclusion

In this paper, we present COMAE for a comprehensive attribute exploration in ZSH. COMAE depicts the relationships between seeable and unseeable classes through meticulously designed explorations: *point-wise*, *pair-wise*, and *class-wise* constraints. Our model employs an attribute prototype network to regress attributes, facilitating the learning of

local features. Then, we employ contrastive learning to capture the context of attributes, moving beyond instance-independent optimization. Finally, we introduce the class-wise constraint to cohesively enhance hashing learning, image representations, and visual attributes. Experiments demonstrate the excellent performance of COMAE.

References

- [1] Andoni, A., Indyk, P., 2008. Near-optimal hashing algorithms for approximate nearest neighbor in high dimensions. *Communications of the ACM* 51, 117–122.
- [2] Arik, S.Ö., Pfister, T., 2019. Attention-based prototypical learning towards interpretable, confident and robust deep neural networks. *arXiv preprint arXiv:1902.06292* .
- [3] Cao, Z., Long, M., Wang, J., Yu, P.S., 2017. Hashnet: Deep learning to hash by continuation, in: *Proceedings of the IEEE international conference on computer vision*, pp. 5608–5617.
- [4] Chen, S., Hong, Z., Liu, Y., Xie, G.S., Sun, B., Li, H., Peng, Q., Lu, K., You, X., 2022. Transzero: Attribute-guided transformer for zero-shot learning, in: *Proceedings of the AAAI Conference on Artificial Intelligence*, pp. 330–338.
- [5] Chen, T., Kornblith, S., Norouzi, M., Hinton, G., 2020. A simple framework for contrastive learning of visual representations, in: *International conference on machine learning*, PMLR. pp. 1597–1607.
- [6] Chen, Y., Yang, Z., Xie, Y., Wang, Z., 2018. Contrastive learning from pairwise measurements. *Advances in Neural Information Processing Systems* 31.
- [7] Fan, L., Ng, K.W., Ju, C., Zhang, T., Chan, C.S., 2020. Deep polarized network for supervised learning of accurate binary hashing codes, in: *IJCAI*, pp. 825–831.
- [8] Farhadi, A., Endres, I., Hoiem, D., Forsyth, D., 2009. Describing objects by their attributes, in: *2009 IEEE conference on computer vision and pattern recognition*, IEEE. pp. 1778–1785.
- [9] Gao, T., Han, X., Liu, Z., Sun, M., 2019. Hybrid attention-based prototypical networks for noisy few-shot relation classification, in: *Proceedings of the AAAI conference on artificial intelligence*, pp. 6407–6414.
- [10] Gong, Y., Lazebnik, S., Gordo, A., Peronnin, F., 2012. Iterative quantization: A procrustean approach to learning binary codes for large-scale image retrieval. *IEEE transactions on pattern analysis and machine intelligence* 35, 2916–2929.
- [11] Guo, Y., Ding, G., Han, J., Gao, Y., 2017. Sitnet: Discrete similarity transfer network for zero-shot hashing, in: *IJCAI*, pp. 1767–1773.
- [12] Hadsell, R., Chopra, S., LeCun, Y., 2006. Dimensionality reduction by learning an invariant mapping, in: *2006 IEEE computer society conference on computer vision and pattern recognition (CVPR'06)*, IEEE. pp. 1735–1742.
- [13] Han, Z., Fu, Z., Chen, S., Yang, J., 2021. Contrastive embedding for generalized zero-shot learning, in: *Proceedings of the IEEE/CVF conference on computer vision and pattern recognition*, pp. 2371–2381.
- [14] Hoe, J.T., Ng, K.W., Zhang, T., Chan, C.S., Song, Y.Z., Xiang, T., 2021. One loss for all: Deep hashing with a single cosine similarity based learning objective. *Advances in Neural Information Processing Systems* 34, 24286–24298.
- [15] Ju, W., Fang, Z., Gu, Y., Liu, Z., Long, Q., Qiao, Z., Qin, Y., Shen, J., Sun, F., Xiao, Z., et al., 2023. A comprehensive survey on deep graph representation learning. *arXiv preprint arXiv:2304.05055* .
- [16] Ju, W., Yi, S., Wang, Y., Long, Q., Luo, J., Xiao, Z., Zhang, M., 2024. A survey of data-efficient graph learning. *arXiv preprint arXiv:2402.00447* .
- [17] Khan, R.U., Zhang, X., Kumar, R., Aboagye, E.O., 2018. Evaluating the performance of resnet model based on image recognition, in: *Proceedings of the 2018 International Conference on Computing and Artificial Intelligence*, pp. 86–90.
- [18] Lew, M.S., Sebe, N., Djeraba, C., Jain, R., 2006. Content-based multimedia information retrieval: State of the art and challenges. *ACM Transactions on Multimedia Computing, Communications, and Applications (TOMM)* 2, 1–19.
- [19] Li, G., Jampani, V., Sevilla-Lara, L., Sun, D., Kim, J., Kim, J., 2021. Adaptive prototype learning and allocation for few-shot segmentation, in: *Proceedings of the IEEE/CVF conference on computer vision and pattern recognition*, pp. 8334–8343.
- [20] Li, Y., van Gemert, J., 2021. Deep unsupervised image hashing by maximizing bit entropy, in: *Proceedings of the AAAI Conference on Artificial Intelligence*, pp. 2002–2010.
- [21] Liu, W., Wen, Y., Yu, Z., Li, M., Raj, B., Song, L., 2017. Sphereface: Deep hypersphere embedding for face recognition, in: *Proceedings of the IEEE conference on computer vision and pattern recognition*, pp. 212–220.
- [22] Long, Q., Jin, Y., Song, G., Li, Y., Lin, W., 2020. Graph structural-topic neural network, in: *Proceedings of the 26th ACM SIGKDD International Conference on Knowledge Discovery & Data Mining*, pp. 1065–1073.
- [23] Long, Q., Xu, L., Fang, Z., Song, G., 2021. Hgk-gnn: Heterogeneous graph kernel based graph neural networks, in: *Proceedings of the 27th ACM SIGKDD Conference on Knowledge Discovery & Data Mining*, pp. 1129–1138.
- [24] Van der Maaten, L., Hinton, G., 2008. Visualizing data using t-sne. *Journal of machine learning research* 9.
- [25] Maćkiewicz, A., Ratajczak, W., 1993. Principal components analysis (pca). *Computers & Geosciences* 19, 303–342.
- [26] Patterson, G., Hays, J., 2012. Sun attribute database: Discovering, annotating, and recognizing scene attributes, in: *2012 IEEE conference on computer vision and pattern recognition*, IEEE. pp. 2751–2758.

- [27] Pourpanah, F., Abdar, M., Luo, Y., Zhou, X., Wang, R., Lim, C.P., Wang, X.Z., Wu, Q.J., 2022. A review of generalized zero-shot learning methods. *IEEE transactions on pattern analysis and machine intelligence* .
- [28] Qiu, Z., Su, Q., Ou, Z., Yu, J., Chen, C., 2021. Unsupervised hashing with contrastive information bottleneck. *arXiv preprint arXiv:2105.06138* .
- [29] Shen, F., Shen, C., Liu, W., Tao Shen, H., 2015a. Supervised discrete hashing, in: *Proceedings of the IEEE conference on computer vision and pattern recognition*, pp. 37–45.
- [30] Shen, F., Shen, C., Shi, Q., Van den Hengel, A., Tang, Z., Shen, H.T., 2015b. Hashing on nonlinear manifolds. *IEEE Transactions on Image Processing* 24, 1839–1851.
- [31] Shen, Y., Qin, J., Chen, J., Liu, L., Zhu, F., Shen, Z., 2019. Embarrassingly simple binary representation learning, in: *Proceedings of the IEEE/CVF International Conference on Computer Vision Workshops*, pp. 0–0.
- [32] Shi, Y., Nie, X., Liu, X., Yang, L., Yin, Y., 2022. Zero-shot hashing via asymmetric ratio similarity matrix. *IEEE Transactions on Knowledge and Data Engineering* 35, 5426–5437.
- [33] Song, G., Long, Q., Luo, Y., Wang, Y., Jin, Y., 2020. Deep convolutional neural network based medical concept normalization. *IEEE Transactions on Big Data* 8, 1195–1208.
- [34] Song, Z., Su, Q., Chen, J., 2023. Unsupervised hashing with contrastive learning by exploiting similarity knowledge and hidden structure of data, in: *Proceedings of the 31st ACM International Conference on Multimedia*, pp. 6350–6358.
- [35] Su, S., Zhang, C., Han, K., Tian, Y., 2018. Greedy hash: Towards fast optimization for accurate hash coding in cnn. *Advances in neural information processing systems* 31.
- [36] Sylvain, T., Petri, L., Hjelm, D., 2019. Locality and compositionality in zero-shot learning. *arXiv preprint arXiv:1912.12179* .
- [37] Tan, Y., Long, G., Liu, L., Zhou, T., Lu, Q., Jiang, J., Zhang, C., 2022. Fedproto: Federated prototype learning across heterogeneous clients, in: *Proceedings of the AAAI Conference on Artificial Intelligence*, pp. 8432–8440.
- [38] Venkatesan, R., Koon, S.M., Jakubowski, M.H., Moulin, P., 2000. Robust image hashing, in: *Proceedings 2000 International Conference on Image Processing* (Cat. No. 00CH37101), IEEE. pp. 664–666.
- [39] Wah, C., Branson, S., Welinder, P., Perona, P., Belongie, S., 2011. The caltech-ucsd birds-200-2011 dataset .
- [40] Wang, F., Cheng, J., Liu, W., Liu, H., 2018. Additive margin softmax for face verification. *IEEE Signal Processing Letters* 25, 926–930.
- [41] Wang, X., Shi, Y., Kitani, K.M., 2017. Deep supervised hashing with triplet labels, in: *Computer Vision–ACCV 2016: 13th Asian Conference on Computer Vision*, Taipei, Taiwan, November 20–24, 2016, Revised Selected Papers, Part I 13, Springer. pp. 70–84.
- [42] Weiss, Y., Torralba, A., Fergus, R., 2008. Spectral hashing. *Advances in neural information processing systems* 21.
- [43] Xian, Y., Lampert, C.H., Schiele, B., Akata, Z., 2018. Zero-shot learning—a comprehensive evaluation of the good, the bad and the ugly. *IEEE transactions on pattern analysis and machine intelligence* 41, 2251–2265.
- [44] Xu, W., Xian, Y., Wang, J., Schiele, B., Akata, Z., 2020. Attribute prototype network for zero-shot learning. *Advances in Neural Information Processing Systems* 33, 21969–21980.
- [45] Xu, Y., Yang, Y., Shen, F., Xu, X., Zhou, Y., Shen, H.T., 2017. Attribute hashing for zero-shot image retrieval, in: *2017 IEEE International Conference on Multimedia and Expo (ICME)*, IEEE. pp. 133–138.
- [46] Yang, Y., Luo, Y., Chen, W., Shen, F., Shao, J., Shen, H.T., 2016. Zero-shot hashing via transferring supervised knowledge, in: *Proceedings of the 24th ACM international conference on Multimedia*, pp. 1286–1295.
- [47] Yu, J., Qiu, H., Chen, D., Zhang, H., 2022. Weighted contrastive hashing, in: *Proceedings of the Asian Conference on Computer Vision*, pp. 3861–3876.
- [48] Yuan, L., Wang, T., Zhang, X., Tay, F.E., Jie, Z., Liu, W., Feng, J., 2020. Central similarity quantization for efficient image and video retrieval, in: *Proceedings of the IEEE/CVF conference on computer vision and pattern recognition*, pp. 3083–3092.
- [49] Zhang, H., Long, Y., Shao, L., 2019. Zero-shot hashing with orthogonal projection for image retrieval. *Pattern Recognition Letters* 117, 201–209.
- [50] Zheng, H., Fu, J., Mei, T., Luo, J., 2017. Learning multi-attention convolutional neural network for fine-grained image recognition, in: *Proceedings of the IEEE international conference on computer vision*, pp. 5209–5217.
- [51] Zheng, S., Gupta, G., 2022. Semantic-guided zero-shot learning for low-light image/video enhancement, in: *Proceedings of the IEEE/CVF Winter conference on applications of computer vision*, pp. 581–590.
- [52] Zhou, C., Po, L.M., Yuen, W.Y., Cheung, K.W., Xu, X., Lau, K.W., Zhao, Y., Liu, M., Wong, P.H., 2019. Angular deep supervised hashing for image retrieval. *IEEE Access* 7, 127521–127532.

Received 10 July 2024; revised 12 August 2024; accepted 5 September 2024